

## Article

# Modulating the Fibrillization of Parathyroid-Hormone (PTH) Peptides: Azo-Switches as Reversible and Catalytic Entities

André Paschold <sup>1</sup>, Bruno Voigt <sup>2</sup>, Gerd Hause <sup>3</sup>, Tim Kohlmann <sup>1</sup>, Sven Rothemund <sup>4</sup> and Wolfgang H. Binder <sup>1,\*</sup>

<sup>1</sup> Department of Chemistry, Faculty of Natural Sciences II, Martin-Luther University Halle-Wittenberg, 06120 Halle (Saale), Germany; andre.paschold@chemie.uni-halle.de (A.P.); tim\_kohlmann@web.de (T.K.)

<sup>2</sup> Department of Physics, Faculty of Natural Sciences II, Martin-Luther University Halle-Wittenberg, 06120 Halle (Saale), Germany; bruno.voigt@physik.uni-halle.de

<sup>3</sup> Biozentrum, Martin-Luther University Halle-Wittenberg, 06120 Halle (Saale), Germany; gerd.hause@biozentrum.uni-halle.de

<sup>4</sup> Core Unit Peptide—Technologies, University Leipzig, 04103 Leipzig, Germany; sven.rothemund@medizin.uni-leipzig.de

\* Correspondence: wolfgang.binder@chemie.uni-halle.de

**Abstract:** We here report a novel strategy to control the bioavailability of the fibrillizing parathyroid hormone (PTH)-derived peptides, where the concentration of the bioactive form is controlled by an reversible, photoswitchable peptide. PTH<sub>1-84</sub>, a human hormone secreted by the parathyroid glands, is important for the maintenance of extracellular fluid calcium and phosphorus homeostasis. Controlling fibrillization of PTH<sub>1-84</sub> represents an important approach for in vivo applications, in view of the pharmaceutical applications for this protein. We embed the azobenzene derivate 3-[[4-aminomethyl)phenyl]diazanyl]benzoic acid (3,4'-AMPB) into the PTH-derived peptide PTH<sub>25-37</sub> to generate the artificial peptide AzoPTH<sub>25-37</sub> via solid-phase synthesis. AzoPTH<sub>25-37</sub> shows excellent photostability (more than 20 h in the dark) and can be reversibly photoswitched between its *cis/trans* forms. As investigated by ThT-monitored fibrillization assays, the *trans*-form of AzoPTH<sub>25-37</sub> fibrillizes similar to PTH<sub>25-37</sub>, while the *cis*-form of AzoPTH<sub>25-37</sub> generates only amorphous aggregates. Additionally, *cis*-AzoPTH<sub>25-37</sub> catalytically inhibits the fibrillization of PTH<sub>25-37</sub> in ratios of up to one-fifth. The approach reported here is designed to control the concentration of PTH-peptides, where the bioactive form can be catalytically controlled by an added photoswitchable peptide.

**Keywords:** azobenzene; photoswitchable peptides; fibrillization; parathyroid hormone; aggregation



**Citation:** Paschold, A.; Voigt, B.; Hause, G.; Kohlmann, T.; Rothemund, S.; Binder, W.H. Modulating the Fibrillization of Parathyroid-Hormone (PTH) Peptides: Azo-Switches as Reversible and Catalytic Entities. *Biomedicines* **2022**, *10*, 1512. <https://doi.org/10.3390/biomedicines10071512>

Academic Editors: Anne Skaja Robinson and Christopher J. Roberts

Received: 23 May 2022

Accepted: 23 June 2022

Published: 26 June 2022

**Publisher's Note:** MDPI stays neutral with regard to jurisdictional claims in published maps and institutional affiliations.



**Copyright:** © 2022 by the authors. Licensee MDPI, Basel, Switzerland. This article is an open access article distributed under the terms and conditions of the Creative Commons Attribution (CC BY) license (<https://creativecommons.org/licenses/by/4.0/>).

## 1. Introduction

Fibrillization of proteins and peptides is a supramolecular process [1,2] that leads to the formation of peptide aggregates, containing a cross- $\beta$ -sheet motif [3]. It involves multiple steps [4] and is associated with many diseases such as Alzheimer's disease, Parkinson's disease or diabetes type II [5–7]. However, in the past decades, it has also been associated with amyloids with distinct physiological functions, so-called functional amyloids, which are found in lower organisms [8–11]. Subsequently, functional amyloids were also discovered in humans, whereby the amyloid can be the active physiological form [12,13] or the storage form of peptide hormones [14].

The parathyroid hormone, abbreviated PTH, is a human hormone secreted by the parathyroid glands [15], with PTH-like peptides also known from other animals [16,17]. It is expressed as a 115 residue pre-pro-protein, whereby the first 25 amino acids at the *N*-terminus (referred to PTH<sub>-31--7</sub>) serve as a signaling peptide for the transport to the endoplasmic reticulum and are removed by a signal peptidase [18]. The formed pro-peptide is subsequently transferred to the Golgi apparatus and the *N*-terminal six amino acids (referred to PTH<sub>-6--1</sub>) are proteolytically removed [19]. Before mature PTH<sub>1-84</sub> is released into the blood, it is stored in secretory granules as amyloid fibrils [20]. The physiological role

is well studied [21,22], being important in the maintenance of extracellular fluid calcium and phosphorus homeostasis. The receptor is mainly activated through the first 34 N-terminal amino acids [23], wherefore recombinant PTH<sub>1–84</sub> and recombinant PTH<sub>1–34</sub> are approved drugs against osteoporosis, Natpara<sup>®</sup> and Forteo<sup>®</sup>, respectively. However, its fibrillization has barely been investigated. Thus far, it is known that the amyloid fibrils of PTH<sub>1–84</sub> are formed by the amino acid residues R25–L37, and the thermodynamic stability of the fibrils is sufficiently low to dissociate after dilution [20]. Thus, control over the fibrillization of amyloids and PTH specifically represents an important approach for controlling its factual concentration for in vivo applications, placing modulators of fibrillization and thus reversible fibrillization into the focus of pharmaceutically applicable proteins [24–27].

In the past decades, the photoinduced switching of protein functionalities has emerged as an important concept to modulate protein function, often by modulations in binding specificity between proteins and ligands. Thus, not only enzymes have been equipped with photosensitive switches, but also larger protein complexes, involved in many physiological or neurological functions [28]. To this end, artificial photoswitches are embedded into either the main chain or side chains of polypeptides, in order to change their secondary structures by photoinduced conformational changes of the photoswitches. Thereby, a plethora of different photoswitches, such as those based on *cis-trans*-isomerization of azo-dyes [29,30] stilbenes [31] and hemithioindigos [32,33], have been developed. Important for the proper use of a specific photoswitch inside a polypeptide chain is not only the quest to retain the initial (functional) secondary structure of the protein, but also to achieve a reasonably stable conformation after photoswitching, so as to allow for sufficient time to exert the desired effect. Many examples of such sufficiently stable and also reversible photoswitches have been reported, allowing one to modulate several aspects of protein function [34–39]. Here, we report on an approach to modulate the fibrillization of PTH, equipped with a photoswitch at a specific position in the peptide sequence, in order to reversibly trigger its aggregation/disaggregation (see Figure 1).

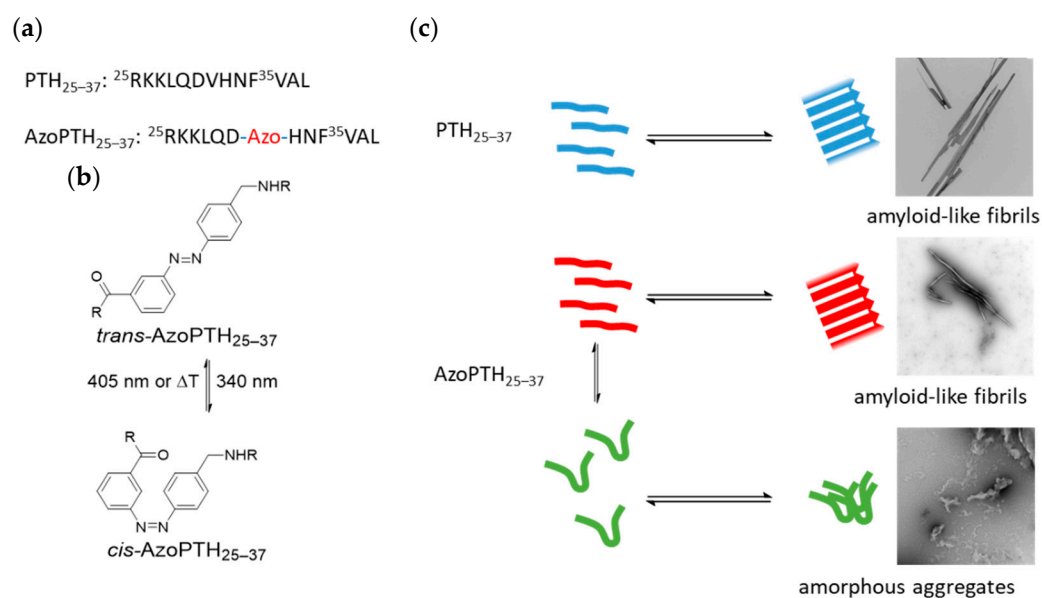


**Figure 1.** (a) Primary sequence of PTH<sub>25–37</sub> and the azobenzene-modified PTH<sub>25–37</sub> (AzoPTH<sub>25–37</sub>, azobenzene-moiety highlighted in red). (b) *Cis-trans*-isomerization of the incorporated 3,4'-AMPB switch. (c) Equilibrium of the monomeric peptides PTH<sub>25–37</sub> and AzoPTH<sub>25–37</sub> in both forms and their aggregates.

In view of the functional design of the modified PTH<sub>25–37</sub>, we sought to embed the photoswitch into a region of the protein where aggregation is still possible, but only in a specific (untriggered) conformation of the photoswitch, whereby fibrillization should be inhibited after the conformational change. As a model system, we chose peptides derived

from the PTH fibril core structure, including the amino acids 25R-37L (Figure 1a) [20], which is able to form fibrils itself. In addition, we investigated the influence of both conformations on the fibrillization of the unmodified peptide. As the photoswitch we chose a structural motif from the class of azobenzenes, as they are well known for enabling reversible control of peptide conformation [29,34,39–41]. Specifically we chose the azobenzene derivate 3-[[4-(4-aminomethyl)phenyl]diazenyl]benzoic acid (3,4'-AMPB; Figure 1b) [42], which is known to introduce a significant geometric change. 3,4'-AMPB displays both: a high photoisomerization yield and a sufficient thermodynamically stability of the *cis*-isomer [41]. If desired, the photoswitch can be reversed via irradiation at 405 nm, or thermally, with a half-life time of more than 20 h in the dark. We hypothesized that the incorporation of the azobenzene into the backbone would allow us to switch between the *cis*- and the *trans*-conformation, whereby one of them is able to fibrillize and the other one is not. Furthermore, azobenzenes in their *cis*-conformation are known to mimic  $\beta$ -hairpins, which allowed us to investigate the hypothesis if the PTH fibrils possess a turn region like amyloid fibrils from other peptides [43–45].

## 2. Materials and Methods

### 2.1. General

All technical solvents were distilled prior to use. Air- and moisture-sensitive reactions were carried out in flame-dried glassware under atmospheric pressure of nitrogen. 2-(6-Chloro-1-H-benzotriazole-1-yl)-1,1,3,3-tetramethylammonium hexafluorophosphate (HCTU), *N*-methyl-morpholine (NMM), *N,N*-dicyclohexylcarbodiimide (DIC), *N*-Hydroxybenzotriazole (HOBT), trifluoroacetic acid, 4-aminobenzylamine, and oxone<sup>®</sup> were purchased from Sigma Aldrich (Taufkirchen, Germany). 9-Fluorenylmethyl-*N*-succinimidylcarbonat (Fmoc-OSu) was received from Fluorochem. 3-Aminobenzoic acid was purchased from Merck (Darmstadt, Germany). All these chemicals were used without further purification.

NMR spectra were recorded on a Varian Gemini 400 or 500 spectrometer (400 MHz or 500 MHz; Agilent Technologies, Waldbronn, Germany) at 27 °C in DMSO-*d*<sub>6</sub> (99.8 Atom%D; Chemotrade, Düsseldorf, Germany) or D<sub>2</sub>O (99.8 Atom%D; Sigma-Aldrich, Taufkirchen, Germany). Chemical shifts are given in ppm and referred to the solvent residual signal (DMSO-*d*<sub>6</sub>:  $\delta$  = 2.50 ppm and  $\delta$  = 39.5 ppm; D<sub>2</sub>O:  $\delta$  = 4.79 ppm). The following abbreviations were used for <sup>1</sup>H- and <sup>13</sup>C-NMR peaks' assignment: s = singlet, d = doublet, t = triplet, td = triplet of doublet, and m = multiplet. MestReNova (version 6.0.2–5475, Mestrelab Research S.L., Santiago de Compostela, Spain) was used for data interpretation.

ESI-ToF mass spectrometry was performed on a Bruker Daltonics microTOF (Bruker Corporation, Billerica, MA, USA). Samples were dissolved in HPLC-grade solvents (MeOH, THF, or mixtures; Sigma Aldrich, Taufkirchen, Germany) at concentrations of 0.1 mg/mL and measured via direct injection with a flow rate of 180  $\mu$ L/h using the positive mode with a capillary voltage of 4.5 kV. The spectra were analyzed with otofControl (version 3.4, Bruker Daltonik, Bremen, Germany).

### 2.2. Organic Synthesis

Fmoc-protected 3,4'-AMPB was synthesized in two steps according to literature procedures [42,46].

### 2.3. Peptide Synthesis and Purification

Solid-phase peptide synthesis was utilized on an automated peptide synthesizer MultiPep RS (Intavis AG, Koeln, Germany) using standard Fmoc-chemistry and preloaded resins. Standard coupling of all protected natural amino acids was performed as single couplings in dimethylformamid (DMF) using 5 equivalents of amino acids, HCTU as coupling reagents, and 10 equivalents of NMM as base for 1 h at room temperature. Special building groups, such as Fmoc-3,4'-AMPB, were coupled with 3 equivalents using DIC and HOBT in DMF/*N*-methyl-2-pyrrolidone (NMP) at room temperature and with gentle shaking in the dark overnight.

The *N*-terminal Fmoc-protecting group was removed by washing the resin with 20% piperidine for 20 min. The final side chain deprotection and cleavage from the resin employed a mixture of trifluoroacetic acid and water (90:10 Vol%) with gentle agitation for 2 h at room temperature.

The crude peptides were purified to >95% purity using preparative RP-HPLC (Gilson, Limburg, Germany). For both analytical and preparative use, the mobile phase was a mixture of water (eluent A) and acetonitrile (eluent B), respectively, each containing 0.1% trifluoroacetic acid. Samples were eluted with a linear gradient from 5% B to 95% B in 15 min for analytical runs and in 90 min for preparative runs on a semipreparative PLRP-S column (300 × 25 mm, 8 μm; Agilent Technologies, Waldbronn, Germany). Finally, all peptides were characterized by analytical HPLC Dionex Ultimate 3000 (Thermo Fisher Scientific, Dreieich, Germany) using a PLRP-S column (150 × 4.6 mm, 3 μm; Agilent Technologies, Waldbronn, Germany) and MALDI-MS (Bruker Microflex LT, Bremen, Germany), which gave the expected [M+H]<sup>+</sup> mass peaks.

#### 2.4. Azobenzene Peptide Photoisomerization

*Trans* → *cis* isomerization was performed by irradiating the dissolved peptide in a 1 cm quartz cuvette for 30 min with light of 340 nm wavelength using a 50 W mercury lamp (VEB) and a 340 nm band pass filter (FB340-10, Thorlabs, Bergkirchen, Germany) under stirring. For *cis* → *trans* isomerization, the dissolved peptide was irradiated with light of 405 nm wavelength using a 1.4 W LED (M405L4, Thorlabs, Bergkirchen, Germany) for 30 min under stirring.

#### 2.5. Aggregation Kinetics

ThT-monitored fibrillization assays of artificial peptides and mixtures with PTH<sub>25-37</sub> were investigated by fluorescence intensity measurements using thioflavin T (ThT) as fluorescent dye. Lyophilized peptides were dissolved in 50 mM Na<sub>2</sub>HPO<sub>4</sub> buffer solution with a pH value of 7.4 in a concentration of 2 mg/mL and kept on ice for the next steps. The samples were centrifuged at 13,000 × *g* rpm for 10 s and the concentrations were determined with a JASCO V-660 absorbance spectrometer (JASCO, Pfungstadt, Germany; PTH<sub>25-37</sub> by absorbance at 205 nm and the molar extinction coefficient of 49,310 cm<sup>-1</sup>M<sup>-1</sup>; *trans*-AzoPTH<sub>25-37</sub> by absorbance at 327 nm and the molar extinction coefficient of 13,000 cm<sup>-1</sup>M<sup>-1</sup>). *Cis*-AzoPTH<sub>25-37</sub> was produced as described before. The solutions were centrifuged at 10,000 rpm for 1 h at 4 °C, the supernatant was transferred to another tube. The protein solutions were mixed in the desired ration and diluted with 50 mM Na<sub>2</sub>HPO<sub>4</sub> buffer (pH 7.4) to obtain final concentrations of 0/100 μM PTH<sub>25-37</sub>, 50 μM ThT, and 0/10/20/50/100 μM AzoPTH<sub>25-37</sub>. For each sample, a total volume of 480 μL was prepared and 3 × 150 μL were transferred to a medium binding 96-well plate (Greiner Bio-One, Kremsmünster, Austria). The plate was sealed with a microplate cover. The fluorescence intensity was monitored at 37 °C using a BMG FLUOStar Omega multi-mode plate reader (BMG LABTECH, Ortenberg, Germany) using fluorescence excitation and emission wavelengths at 460 nm and 485 nm, respectively. One measurement cycle of 5 min consisted of double-orbital shaking for 150 s and incubating for 150 s.

#### 2.6. Transmission Electron Microscopy (TEM)

TEM images were taken with an electron microscope (EM 900; Zeiss, Oberkochen, Germany) at 80 kV acceleration voltage. For preparation, 5 μL of the peptide solution were added on Formvar/Cu grids (mesh 200). After 3 min of incubation, the grids were gently cleaned with water for 0.1 min and then negatively stained using uranyl acetate (1%, *w/v*) for 1 min.

#### 2.7. Seeding Assay

The seeding assay follows the same procedure as the ThT-monitored fibrillization assay for the determination of the aggregation kinetics. In addition, the final samples

contained 20  $\mu\text{M}$  of seeds from *trans*-AzoPTH<sub>25–37</sub> fibrils. The seeds were prepared via ultrasonication of a 100  $\mu\text{M}$  mature *trans*-AzoPTH<sub>25–37</sub> fibrils solution (Sonifier W-250 D, Branson Ultraschall, Dietzenbach, Germany; 15 times, 1 s 10% amplitude, 1 s pause).

### 3. Results & Discussion

#### 3.1. Chemistry

To investigate the fibrillization behavior of PTH<sub>25–37</sub>, the azobenzene switch was incorporated directly into the peptide backbone. We selected the 3,4'-azobenzene motif (Figure 1b) [42]. As it possesses suitable photochemical properties, e.g., an excellent half-life time with a stability larger than 20 h and switching wavelengths >300 nm. These are easily addressable by our photophysical equipment and also avoid eventual photodegradation. The synthesis was conducted in two steps (Figure 2a): in the first step, we conducted the Fmoc-protection of **2** [46], which in the second step reacts in a Mills reaction with an in situ-generated nitroso compound **3** to obtain the Fmoc-protected 3,4'-AMPB **5** in an overall yield of 68%.

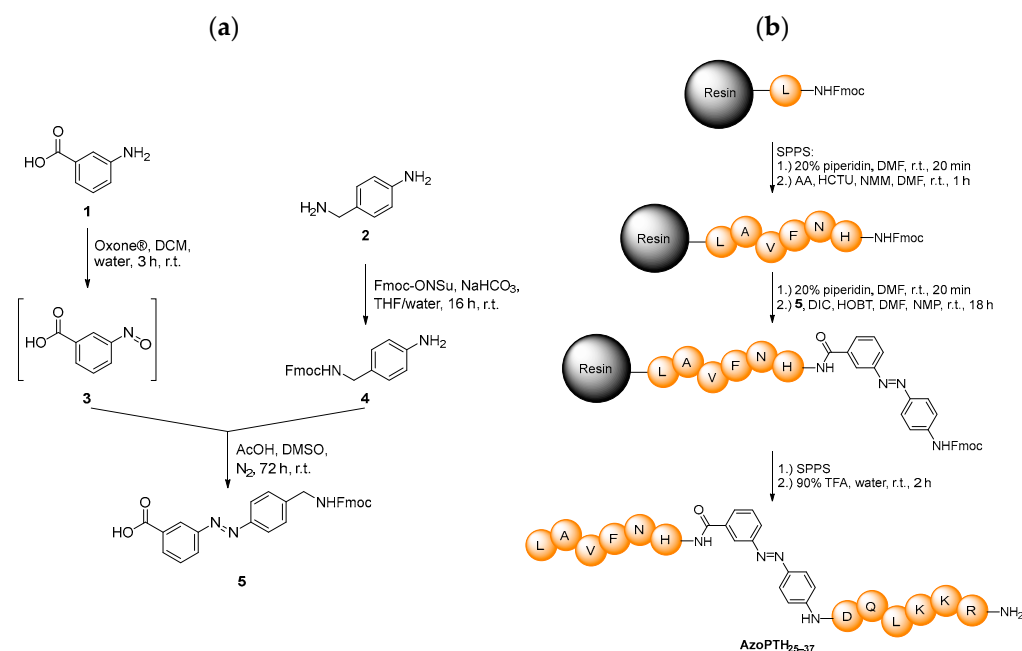


**Figure 2.** (a) Synthesis of Fmoc-protected *trans*-3,4'-AMPB **5**. (b) Solid-phase peptide synthesis strategy towards the peptide AzoPTH<sub>25–37</sub>.

The modified azobenzene switch **5**, bearing the proper functionalities for Fmoc-chemistry, was incorporated into the peptide backbone of PTH<sub>25–37</sub> via solid-phase peptide synthesis (Figure 2b). It replaces V31 in the artificial peptide AzoPTH<sub>25–37</sub>, due to its central position along the peptide, expecting the largest impact on fibrillization after photoswitching. Furthermore, we probed the replacement of D30 or the insertion between D30 and V31, which led to a greater loss of solubility in the fibrillization buffer (240  $\mu\text{M}$  vs. 25  $\mu\text{M}$  vs. 60  $\mu\text{M}$ ; Table S1). Thus, several of the generated peptides displayed strongly reduced solubility—an effect that is important for the subsequent investigations. All peptides were obtained in yields of 10–19%, and high purities as proven by both HPLC and MALDI-ToF measurements, in addition to 500 MHz NMR spectroscopy (Figures S1–S5 and S13–S15).

#### 3.2. Photophysical Properties

We first studied the photophysical properties of the *cis-trans*-isomerization of AzoPTH<sub>25–37</sub> (Figure 1b) by UV/Vis spectroscopy and HPLC analysis in pure water in order to minimize effects of a potential self-assembly and to quantify the generated amounts of the respective *cis/trans*-modified peptides before and after photoswitching. The UV/Vis spectra for the

pure isomers (Figure S6) were separated from the spectra of *trans*-enriched AzoPTH<sub>25–37</sub> in the thermodynamically stable state after synthesis and in the *cis*-enriched photostationary state (PSS, Figure 3) with Wolfram Mathematica 12.2. The *trans*-isomer displays an absorption maximum at 327 nm ( $\epsilon = 13,000 \text{ cm}^{-1}\text{M}^{-1}$ ) and a second maximum at 427 nm, while the *cis*-isomer possesses maxima at 288 nm and 433 nm. Both isomers display two isobestic points at 278 nm and 388 nm. They represent in the thermodynamically stable state a *cis-trans* ratio of 3:97. Under irradiation with UV light (340 nm), the *cis*-content could be increased of up to 82% in the *cis*-enriched PSS. Visible light (405 nm) yields 76% of the *trans*-isomer in the *trans*-enriched PSS via the back reaction. The difference of the *trans*-content between the *trans*-enriched PSS at 405 nm and the thermodynamically stable state arises from the overlapping of the  $n \rightarrow \pi^*$  transitions of both isomers at this wavelength [47]. The rate of thermal *cis*-to-*trans* isomerization of AzoPTH<sub>25–37</sub> follows first-order kinetics, and was determined by monitoring the increase of the  $\pi \rightarrow \pi^*$  absorption band at 327 nm (Figure S7) via time-dependent UV measurements. In the absence of light at 37 °C, *cis*-AzoPTH<sub>25–37</sub> isomerizes thermally with a rate constant of  $3.53 \times 10^{-6} \text{ s}^{-1}$ , corresponding to a half-life time of 79 h.

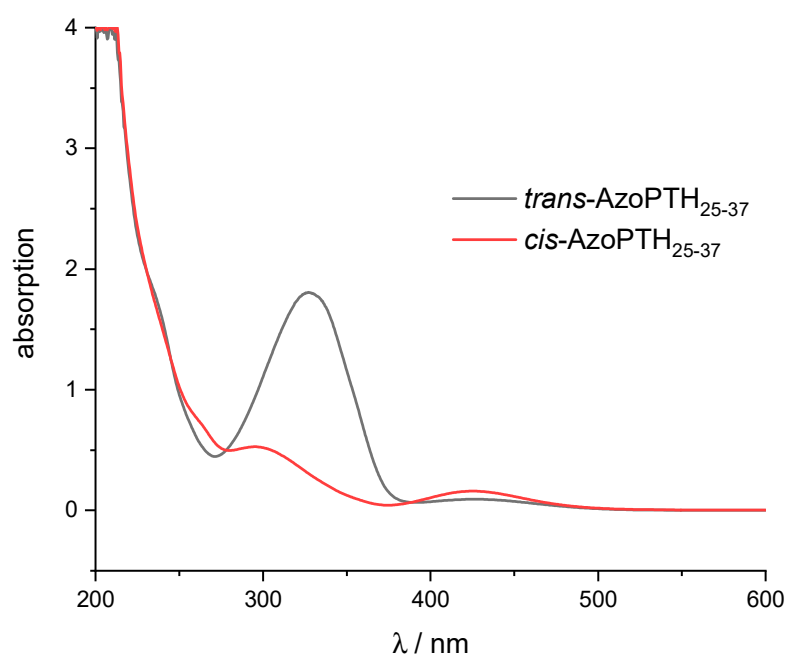


**Figure 3.** UV/Vis absorption spectra for *trans*-AzoPTH<sub>25–37</sub> after synthesis and for the *cis*-enriched photo-stationary state after irradiation at 340 nm, which almost corresponds to *cis*-AzoPTH<sub>25–37</sub>.

### 3.3. Aggregation Kinetics and TEM-Recordings

In order to determine the kinetics of fibril formation of both modified AzoPTH<sub>25–37</sub> isomers a thioflavin T (ThT)-monitored fibrillization assay was conducted and compared to PTH<sub>25–37</sub>. ThT is a benzothiazole compound that binds to the cross- $\beta$ -sheet structure of amyloid fibrils [48]. Causing a large red shift of fluorescence excitation of ThT, which in turn enables the selective excitation of amyloid fibril-bound ThT and therefore the in situ observation of fibril formation.

In a first attempt, the fibrillization kinetics for pure *trans*-AzoPTH<sub>25–37</sub>, *cis*-AzoPTH<sub>25–37</sub>, and the PTH-derived peptide PTH<sub>25–37</sub> were measured at 37 °C and the results are shown in Figure 4. Two characteristic times were used to characterize the fibrillization (Figure 4, Table 1): the lag time  $t_{\text{lag}}$  corresponds to the time before an increase in the fluorescence signal occurs; the characteristic time  $t_{\text{char}}$  indicates at which time 50% of the maximum fluorescence was reached.

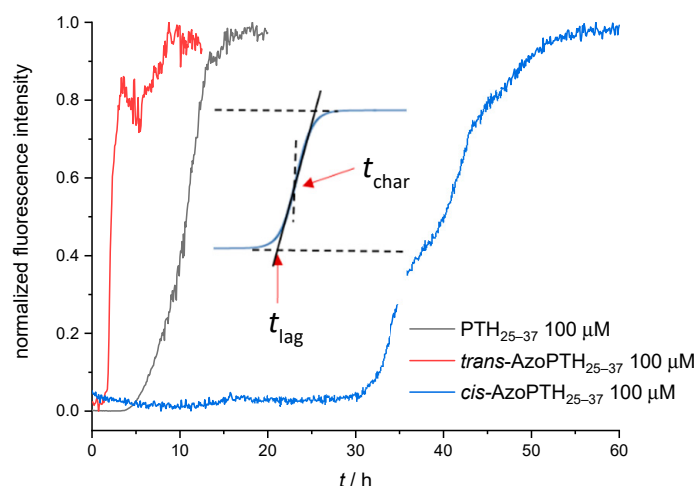


**Figure 4.** ThT-monitored fibrillization assay of PTH<sub>25–37</sub>, *cis*-AzoPTH<sub>25–37</sub>, and *trans*-AzoPTH<sub>25–37</sub> (average of triplets;  $T = 37\text{ }^{\circ}\text{C}$ , buffer = 50 mM Na<sub>2</sub>HPO<sub>4</sub>, pH = 7.4): (black) PTH<sub>25–37</sub> (100  $\mu\text{M}$ ), (red) *trans*-AzoPTH<sub>25–37</sub> (100  $\mu\text{M}$ ), and (blue) *cis*-AzoPTH<sub>25–37</sub> (100  $\mu\text{M}$ ).

**Table 1.** Fibrillization parameters ( $t_{\text{lag}}$ ,  $t_{\text{char}}$ ) of PTH<sub>25–37</sub>, *cis*-AzoPTH<sub>25–37</sub>, *trans*-AzoPTH<sub>25–37</sub>, and mixtures thereof ( $T = 37\text{ }^{\circ}\text{C}$ , buffer = 50 mM Na<sub>2</sub>HPO<sub>4</sub>, pH = 7.4).

Sample	$t_{\text{lag}}$ [h]	$t_{\text{char}}$ [h]
PTH <sub>25–37</sub> (100 $\mu\text{M}$ )	7.2	10.9
<i>cis</i> -AzoPTH <sub>25–37</sub> (100 $\mu\text{M}$ )	34.4	42.4
<i>cis</i> -AzoPTH <sub>25–37</sub> :PTH <sub>25–37</sub> (100 $\mu\text{M}$ :100 $\mu\text{M}$ )	27.9	35.7
<i>cis</i> -AzoPTH <sub>25–37</sub> :PTH <sub>25–37</sub> (50 $\mu\text{M}$ :100 $\mu\text{M}$ )	16.3	21.2
<i>cis</i> -AzoPTH <sub>25–37</sub> :PTH <sub>25–37</sub> (20 $\mu\text{M}$ :100 $\mu\text{M}$ )	10.1	14.5
<i>cis</i> -AzoPTH <sub>25–37</sub> :PTH <sub>25–37</sub> (10 $\mu\text{M}$ :100 $\mu\text{M}$ )	6.9	7.9
<i>trans</i> -AzoPTH <sub>25–37</sub> (100 $\mu\text{M}$ )	1.6	2.1
<i>trans</i> -AzoPTH <sub>25–37</sub> :PTH <sub>25–37</sub> (100 $\mu\text{M}$ :100 $\mu\text{M}$ )	3.0	4.8
<i>trans</i> -AzoPTH <sub>25–37</sub> :PTH <sub>25–37</sub> (50 $\mu\text{M}$ :100 $\mu\text{M}$ )	8.0	8.6
<i>trans</i> -AzoPTH <sub>25–37</sub> :PTH <sub>25–37</sub> (20 $\mu\text{M}$ :100 $\mu\text{M}$ )	8.7	9.7
<i>trans</i> -AzoPTH <sub>25–37</sub> :PTH <sub>25–37</sub> (10 $\mu\text{M}$ :100 $\mu\text{M}$ )	7.5	8.9

The self-assembly of the *trans*-AzoPTH<sub>25–37</sub> was accelerated compared to PTH<sub>25–37</sub>, while *cis*-AzoPTH<sub>25–37</sub> exhibited the opposite effect (Figure 4). The first increase of ThT fluorescence was observable after >30 h. Furthermore, *cis*-AzoPTH<sub>25–37</sub> shows a biphasic fibrillization behavior, while *trans*-AzoPTH<sub>25–37</sub> and PTH<sub>25–37</sub> show monophasic fibrillization. Compared to PTH<sub>25–37</sub>, the magnitude of the ThT fluorescence of both AzoPTH<sub>25–37</sub> isomers was significant lower (Figure S9). This effect might arise from fluorescence quenching via the azobenzene moiety. To test this hypothesis, the fluorescence lifetime of ThT was measured either alone, in the presence of PTH<sub>25–37</sub> fibrils, or in the presence of *trans*-AzoPTH<sub>25–37</sub> fibrils (Figure S8). As expected the lifetime is increased in the presence of PTH<sub>25–37</sub> fibrils compared to the control experiment, while it is decreased significantly in the presence of *trans*-AzoPTH<sub>25–37</sub>, which further supports our concept. In addition, this effect could be enhanced from a reduced binding affinity of ThT through a different peptide conformation of the fibril.

The observations of the ThT-monitored fibrillization assay were supported by negative stain transmission electron microscopy (TEM) after different time points (Figure 5). After 20 h, amyloid fibrils were only observable for PTH<sub>25–37</sub> and *trans*-AzoPTH<sub>25–37</sub> (Figure 5a,b), while *cis*-AzoPTH<sub>25–37</sub> formed amorphous aggregates (Figure 5e). Both peptides produced straight fibrils, whereby the single fibrils of PTH<sub>25–37</sub> were larger (>6  $\mu\text{m}$  vs. <1.5  $\mu\text{m}$ ) and tend to aggregate further. Interestingly, we found fibrils after 60 h for *cis*-AzoPTH<sub>25–37</sub> (Figure 5g), which matched in the morphology those of *trans*-AzoPTH<sub>25–37</sub> even if they were

significantly shorter (<300 nm). This may result from the thermal *cis-trans*-isomerization, as the *cis*-content decreases and is reduced to 48% after 60 h.

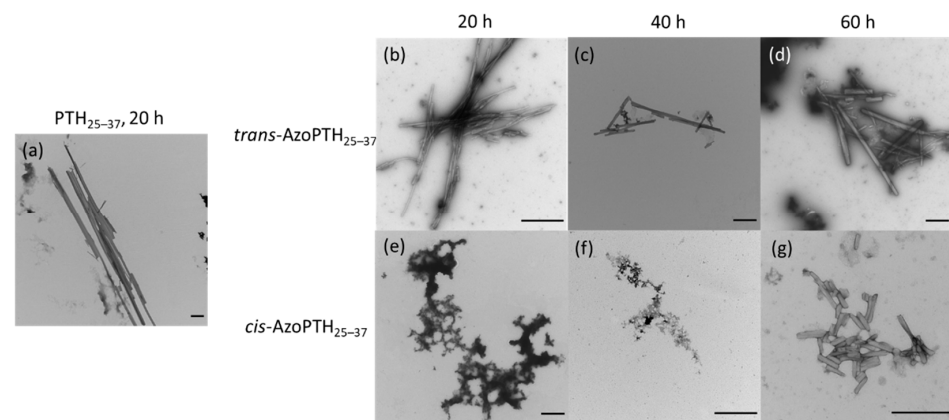


**Figure 5.** TEM recordings of fibrils obtained from PTH<sub>25-37</sub>, *cis*-AzoPTH<sub>25-37</sub>, and *trans*-AzoPTH<sub>25-37</sub> at ( $T = 37\text{ }^{\circ}\text{C}$ , buffer = 50 mM Na<sub>2</sub>HPO<sub>4</sub>, pH = 7.4) after different time points (all scale bars corresponds to 500 nm). (a) PTH<sub>25-37</sub> after 20 h, (b) *trans*-AzoPTH<sub>25-37</sub> after 20 h (100  $\mu\text{M}$ ), (c) *trans*-AzoPTH<sub>25-37</sub> after 40 h (100  $\mu\text{M}$ ), (d) *trans*-AzoPTH<sub>25-37</sub> after 60 h (100  $\mu\text{M}$ ), (e) *cis*-AzoPTH<sub>25-37</sub> after 20 h (100  $\mu\text{M}$ ), (f) *cis*-AzoPTH<sub>25-37</sub> after 40 h (100  $\mu\text{M}$ ), and (g) *cis*-AzoPTH<sub>25-37</sub> after 60 h (100  $\mu\text{M}$ ).

In further experiments, we investigated the (catalytic) influence of the AzoPTH<sub>25-37</sub> isomers on the fibrillization of PTH<sub>25-37</sub> (Figure 6). We previously observed such catalytic effects of  $\beta$ -turn modified amyloids (A $\beta$ ) on the fibrillization of the Alzheimer peptide A $\beta$ <sub>1-40</sub> [49]. Thus 100  $\mu\text{M}$  of PTH<sub>25-37</sub> were fibrillized in the presence of various concentrations of the respective AzoPTH<sub>25-37</sub> isomer (10/20/50/100  $\mu\text{M}$ ). Kinetic measurements revealed that the fibrillization behavior of PTH<sub>25-37</sub> was affected in the same way as the pure AzoPTH<sub>25-37</sub> isomers.

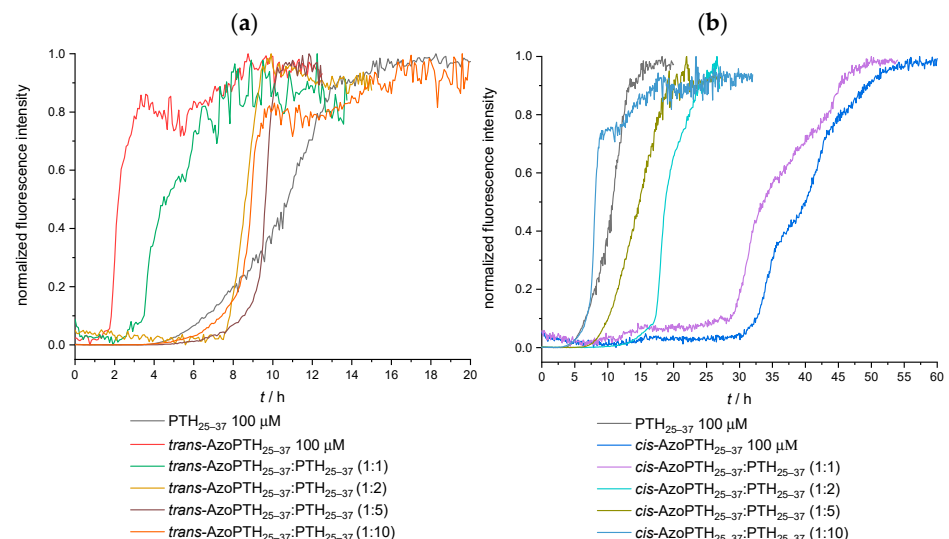


**Figure 6.** (a) ThT-monitored fibrillization assay of PTH<sub>25-37</sub> and mixtures with *trans*-AzoPTH<sub>25-37</sub> (average of triplets;  $T = 37\text{ }^{\circ}\text{C}$ , buffer = 50 mM Na<sub>2</sub>HPO<sub>4</sub>, pH = 7.4): (black) PTH<sub>25-37</sub> (100  $\mu\text{M}$ ), (red) *trans*-AzoPTH<sub>25-37</sub> (100  $\mu\text{M}$ ), (green) *trans*-AzoPTH<sub>25-37</sub>:PTH<sub>25-37</sub> (100  $\mu\text{M}$ :100  $\mu\text{M}$ ), (dark yellow) *trans*-AzoPTH<sub>25-37</sub>:PTH<sub>25-37</sub> (50  $\mu\text{M}$ :100  $\mu\text{M}$ ), (brown) *trans*-AzoPTH<sub>25-37</sub>:PTH<sub>25-37</sub> (20  $\mu\text{M}$ :100  $\mu\text{M}$ ), and (orange) *trans*-AzoPTH<sub>25-37</sub>:PTH<sub>25-37</sub> (10  $\mu\text{M}$ :100  $\mu\text{M}$ ) (b) ThT-monitored fibrillization assay of PTH<sub>25-37</sub> and mixtures with *cis*-AzoPTH<sub>25-37</sub> at 37  $^{\circ}\text{C}$ : (black) PTH<sub>25-37</sub> (100  $\mu\text{M}$ ), (blue) *cis*-AzoPTH<sub>25-37</sub> (100  $\mu\text{M}$ ), (purple) *cis*-AzoPTH<sub>25-37</sub>:PTH<sub>25-37</sub> (100  $\mu\text{M}$ :100  $\mu\text{M}$ ), (cyan) *cis*-AzoPTH<sub>25-37</sub>:PTH<sub>25-37</sub> (50  $\mu\text{M}$ :100  $\mu\text{M}$ ), (olive) *cis*-AzoPTH<sub>25-37</sub>:PTH<sub>25-37</sub> (20  $\mu\text{M}$ :100  $\mu\text{M}$ ), and (light blue) *cis*-AzoPTH<sub>25-37</sub>:PTH<sub>25-37</sub> (10  $\mu\text{M}$ :100  $\mu\text{M}$ ).

While *trans*-AzoPTH<sub>25–37</sub> accelerated the fibrillization and therefore reduced  $t_{lag}$  and  $t_{char}$  of the mixtures (Figure 6a), *cis*-AzoPTH<sub>25–37</sub> inhibited the fibrillization and extended  $t_{lag}$  and  $t_{char}$  (Figure 6b). Interestingly, the biphasic fibrillization behavior of *cis*-AzoPTH<sub>25–37</sub> was also observable for the *cis*-AzoPTH<sub>25–37</sub>:PTH<sub>25–37</sub> (100  $\mu$ M:100  $\mu$ M) mixture. These effects are reduced with decreasing concentration of the respective AzoPTH<sub>25–37</sub> isomer. While the mixtures with *trans*-AzoPTH<sub>25–37</sub> exhibited a concentration below 50  $\mu$ M, *trans*-AzoPTH<sub>25–37</sub> had a higher  $t_{lag}$  than pure PTH<sub>25–37</sub>. However,  $t_{char}$  was still shorter, and the stationary phase of the fibrillization was reached earlier.

TEM images were recorded for the peptide mixtures after 20 h (Figure 7). In contrast to the pure peptides, we could observe fibrils for all investigated ratios. Interestingly, the fibrils formed by the mixtures exhibit a similar twisted morphology regardless of the used AzoPTH<sub>25–37</sub> isomer. Furthermore, the formation of larger aggregates like for the pure PTH<sub>25–37</sub> (Figure 5) were only observed for a ratio of 1:10, indicating that the AzoPTH<sub>25–37</sub> inhibits the formation of larger fibril aggregates.

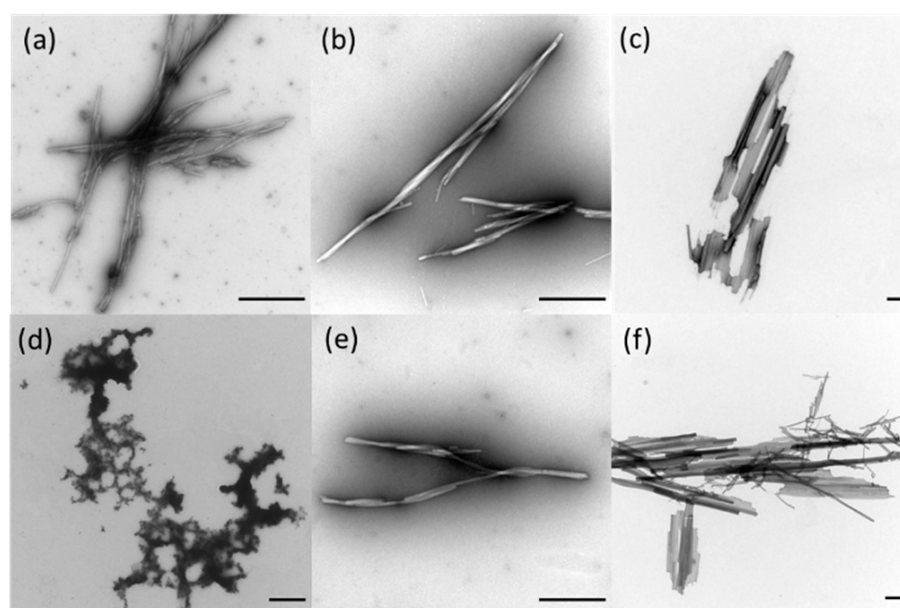


**Figure 7.** TEM recordings of fibrils obtained from PTH<sub>25–37</sub>, *cis*-AzoPTH<sub>25–37</sub>, and *trans*-AzoPTH<sub>25–37</sub> at 37 °C after 20 h (scale bar = 500 nm): (a) *trans*-AzoPTH<sub>25–37</sub> (100  $\mu$ M), (b) *trans*-AzoPTH<sub>25–37</sub>:PTH<sub>25–37</sub> (100  $\mu$ M:100  $\mu$ M), (c) *trans*-AzoPTH<sub>25–37</sub>:PTH<sub>25–37</sub> (10  $\mu$ M:100  $\mu$ M), (d) *cis*-AzoPTH<sub>25–37</sub> (100  $\mu$ M), (e) *cis*-AzoPTH<sub>25–37</sub>:PTH<sub>25–37</sub> (100  $\mu$ M:100  $\mu$ M), and (f) *cis*-AzoPTH<sub>25–37</sub>:PTH<sub>25–37</sub> (10  $\mu$ M:100  $\mu$ M).

### 3.4. Seeding Experiments

To determine whether both isomers of AzoPTH<sub>25–37</sub> are able to form fibrils or only the *trans*-isomer, we investigated, if *trans*-AzoPTH<sub>25–37</sub> fibrils were able to induce seeding [50]. A 100  $\mu$ M solution of each isomer was treated with 20  $\mu$ M of mature *trans*-AzoPTH<sub>25–37</sub> fibrils, and the kinetics of the fibril formation were investigated via a ThT-monitored fibrillization assay (Figure 8). While the fibrillization of the *trans*-isomer was accelerated compared to the unseeded monomer, we were not able to observe fibrillization for the *cis*-isomer. This indicates that the *cis*-isomer is unable to nucleate amyloid formation as well as elongate preformed fibrils. The observed fibrils after 60 h for the *cis*-isomer are presumably formed by the thermally isomerized *trans*-isomer.

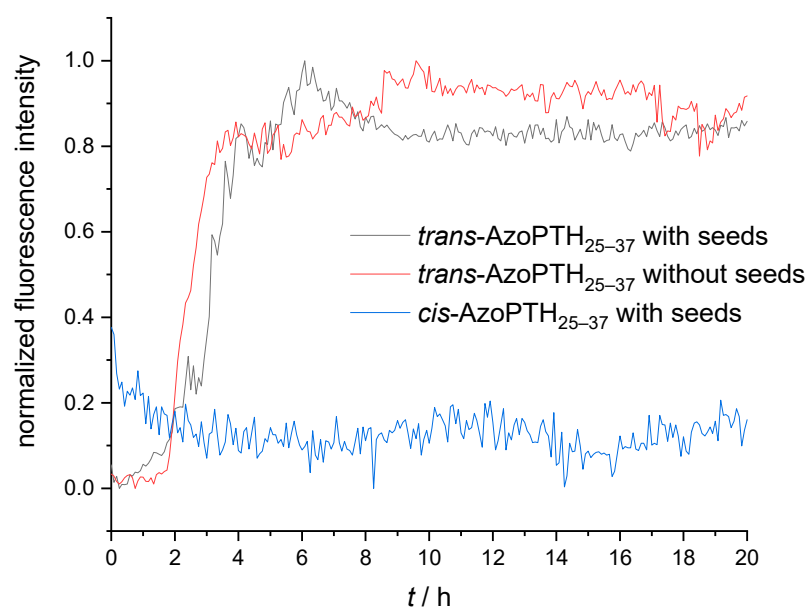


**Figure 8.** ThT-monitored fibrillization assay of cross-seeding studies with *cis*-AzoPTH<sub>25–37</sub> and *trans*-AzoPTH<sub>25–37</sub> monomeric peptides and mature *trans*-AzoPTH<sub>25–37</sub> fibrils as seeds (average of triplets;  $c_{\text{monomer}} = 100 \mu\text{M}$ ,  $c_{\text{seed}} = 20 \mu\text{M}$ ,  $T = 37 \text{ }^\circ\text{C}$ , buffer 50 mM Na<sub>2</sub>HPO<sub>4</sub>, pH = 7.4): (black) *trans*-AzoPTH<sub>25–37</sub> with seeds, (red) *trans*-AzoPTH<sub>25–37</sub> without seeds, and (blue) *cis*-AzoPTH<sub>25–37</sub> with seeds.

#### 4. Conclusions

We here report for the first time a photoswitchable fibrillizing PTH-derived peptide, which is able to modulate its fibrillization by embedding an azobenzene photoswitch in the middle of PTH<sub>25–37</sub>. PTH<sub>1–84</sub> is a peptide hormone, which is stored as functional amyloids in secretory granules. Its physiological role is well studied, but it still lacks detailed information about its exact fibril structure. We used the 3,4'-AMPB photoswitch to investigate the fibril formation of the fibril core fragment of PTH<sub>1–84</sub> by incorporating the azobenzene into the peptide backbone, yielding the modified PTH-derived peptide AzoPTH<sub>25–37</sub>. We could show that the *trans*-isomer is able to form fibrils, while the *cis*-isomer induces a conformational change that inhibits fibril formation. Hypothetically, we can also conclude that there might not be a  $\beta$ -turn in the fibril structure of PTH<sub>1–84</sub>, as the *cis*-conformer would be reminiscent of such a structure, whereas the *trans*-conformer would not. Most importantly, we were able to show that the modified peptides can catalytically inhibit fibrillization of the PTH<sub>25–37</sub>, underscoring the importance of seeding during this fibrillization process, which in the future allows for a reversible triggering of the fibrillization by light as an external stimulus. Studies are in progress to investigate if the photocontrol is also possible with the photoswitch at other positions of the backbone and if we can also control the fibrillization of full-length PTH<sub>1–84</sub> with ours or other modified peptides. This represents a novel strategy to control bioavailability of proteins, specifically of PTH peptides and other fibrillating peptides, where not only the concentration of the bioactive form can be controlled by an added photoswitchable peptide, but also the fibrillization as such, important to guide nerve cell regeneration and other directed growth processes in euryotic cells. For a potential clinical perspective, we want to investigate the cytotoxicity of our peptides as well as the ability to influence the fibrillization of larger PTH-derived peptides (e.g., PTH<sub>1–34</sub> and PTH<sub>1–84</sub>) in vitro and in vivo. As known from other azobenzene containing drugs/prodrugs (e.g., Prontosil), the azobenzene moiety is metabolized in liver tissue via azoreductases, yielding two aniline moieties or through intestinal microbes [51,52]. This is potentially important for the photoswitching inside cells by light, allowing them to tune the reversible fibrillization of other amyloidogenic peptides, which important for regeneration of nerve cells, as reported earlier. Thus, peptide fibrils

can seed potential harmful amyloidogenic peptides, which is known from recent work quite prominently [53]. This is a strategy to trigger fiber-formation from the outside via photochemical triggering—thus avoiding the toxic effects of the fibers outside the cells but enabling triggered fibrillization inside the cell to exert the desired effects, allowing them to promote the recovery of spinal cord injuries.

**Supplementary Materials:** The following supporting information can be downloaded at: <https://www.mdpi.com/article/10.3390/biomedicines10071512/s1>, Figure S1: (A) HPLC-trace of AzoPTH<sub>25–37</sub> (*cis*-isomer at 5.353, *trans*-isomer at 5.530). (B) MALDI-spectrum of AzoPTH<sub>25–37</sub>; Figure S2: (A) HPLC-trace of SP1 (*cis*-isomer at 5.557, *trans*-isomer at 5.790). (B) MALDI-spectrum of SP1; Figure S3: (A) HPLC-trace of SP2 (*cis*-isomer at 5.223, *trans*-isomer at 5.460). (B) MALDI-spectrum of SP2; Figure S4: (A) HPLC-trace of SP3 (*cis*-isomer at 5.560, *trans*-isomer at 5.807). (B) MALDI-spectrum of SP3; Figure S5: (A) HPLC-trace of SP4 (*cis*-isomer at 5.363, *trans*-isomer at 5.547). (B) MALDI-spectrum of SP4; Figure S6: Separated UV/Vis-spectra of the pure isomers of AzoPTH<sub>25–37</sub>; spectra were separated with Wolfram Mathematica 12.2; Figure S7: (A) UV/Vis-spectra of *trans*-isomer, *cis*-enriched PSS, and *cis*-enriched PSS sample after distinct time points in the dark. (B) logarithmic application of the absorption change over time to determine rate constant  $k$  and half-life time  $t_{1/2}$ ; Figure S8: Time-resolved fluorescence measurement (excitation wavelength = 460 nm, emission wavelength = 480 nm) of unbound ThT (black), ThT bound to PTH<sub>25–37</sub> fibrils (dark green), ThT bound to *trans*-AzoPTH<sub>25–37</sub> fibrils (light green); Figure S9: ThT monitored fibrillation assays ( $c = 100 \mu\text{M}$ ,  $37^\circ\text{C}$ ,  $50 \text{ mM Na}_2\text{HPO}_4$ ,  $\text{pH } 7.4$ ). (A) PTH<sub>25–37</sub>, (B) *trans*-AzoPTH<sub>25–37</sub>, (C) *cis*-AzoPTH<sub>25–37</sub>; Figure S10: ThT monitored fibrillation assays of mixtures of PTH<sub>25–37</sub>, *trans*-AzoPTH<sub>25–37</sub>, and *cis*-AzoPTH<sub>25–37</sub> ( $37^\circ\text{C}$ ,  $50 \text{ mM Na}_2\text{HPO}_4$ ,  $\text{pH } 7.4$ ). (A) *trans*-AzoPTH<sub>25–37</sub>:PTH<sub>25–37</sub> (100  $\mu\text{M}$ :100  $\mu\text{M}$ ), (B) *cis*-AzoPTH<sub>25–37</sub>:PTH<sub>25–37</sub> (100  $\mu\text{M}$ :100  $\mu\text{M}$ ), (C) *trans*-AzoPTH<sub>25–37</sub>:PTH<sub>25–37</sub> (50  $\mu\text{M}$ :100  $\mu\text{M}$ ), (D) *cis*-AzoPTH<sub>25–37</sub>:PTH<sub>25–37</sub> (50  $\mu\text{M}$ :100  $\mu\text{M}$ ), (E) *trans*-AzoPTH<sub>25–37</sub>:PTH<sub>25–37</sub> (20  $\mu\text{M}$ :100  $\mu\text{M}$ ), (F) *cis*-AzoPTH<sub>25–37</sub>:PTH<sub>25–37</sub> (20  $\mu\text{M}$ :100  $\mu\text{M}$ ), (G) *trans*-AzoPTH<sub>25–37</sub>:PTH<sub>25–37</sub> (10  $\mu\text{M}$ :100  $\mu\text{M}$ ), (H) *cis*-AzoPTH<sub>25–37</sub>:PTH<sub>25–37</sub> (10  $\mu\text{M}$ :100  $\mu\text{M}$ ); Figure S11:  $^1\text{H}$ -NMR spectrum (top; 400 MHz, DMSO- $d_6$ ) and  $^{13}\text{C}$ -NMR spectrum (bottom; 100 MHz, DMSO- $d_6$ ) of (9*H*-Fluoren-9-yl)methyl (4-aminobenzyl)carbamate; Figure S12:  $^1\text{H}$ -NMR spectrum (top; 400 MHz, DMSO- $d_6$ ) and  $^{13}\text{C}$ -NMR spectrum (bottom; 100 MHz, DMSO- $d_6$ ) of Fmoc-3,4'-AMPB (mixture of isomers); Figure S13:  $^1\text{H}$ -NMR spectra (500 MHz, D<sub>2</sub>O) of AzoPTH<sub>25–37</sub> (top, *trans*-isomer) and SP1 (bottom, *trans*-isomer); Figure S14:  $^1\text{H}$ -NMR spectra (500 MHz, D<sub>2</sub>O) of SP2 (top, *trans*-isomer) and SP3 (bottom, *trans*-isomer); Figure S15:  $^1\text{H}$ -NMR spectrum (500 MHz, D<sub>2</sub>O) of SP4 (*trans*-isomer); Scheme S1: Synthesis of Fmoc-protected 3,4'-AMPB 7. (a) Fmoc-ONSu, triethylamin, DMF/MeCN, 16 h, room temperature. (b) Oxone<sup>®</sup>, DCM, water, 3 h, room temperature. (c) AcOH, DMSO, N<sub>2</sub>, 72 h, room temperature; Table S1: Primary sequence and solubility in 50 mM Na<sub>2</sub>HPO<sub>4</sub> buffer (pH 7.4) of peptides AzoPTH<sub>25–37</sub> and SP1–SP4.

**Author Contributions:** Conceptualization, A.P. and W.H.B.; methodology, A.P., B.V., G.H., T.K. and S.R.; validation, A.P. and B.V.; investigation, A.P.; writing—original draft preparation, A.P.; writing—review and editing, A.P. and W.H.B.; supervision, W.H.B.; project administration, W.H.B.; funding acquisition, W.H.B. All authors have read and agreed to the published version of the manuscript.

**Funding:** This research was funded by DFG—Deutsche Forschungsgemeinschaft, Project ID 189853844—TRR 102, TP A12.

**Institutional Review Board Statement:** Not applicable.

**Informed Consent Statement:** Not applicable.

**Data Availability Statement:** Data are contained within the article.

**Acknowledgments:** The authors thank Jochen Balbach (Martin Luther University Halle-Wittenberg, Department of Physics) and Maria Ott (Martin Luther University Halle-Wittenberg, Department of Biochemistry and Biotechnology) for the use of equipment, their advice, and for discussions.

**Conflicts of Interest:** The authors declare no conflict of interest. The funders had no role in the design of the study; in the collection, analyses, or interpretation of data; in the writing of the manuscript, or in the decision to publish the results.

## References

1. Hamley, I.W. Peptide fibrillization. *Angew. Chem. Int. Ed.* **2007**, *46*, 8128–8147. [[CrossRef](#)] [[PubMed](#)]
2. Binder, W.H.; Smrzka, O.W. Self-Assembly of Fibers and Fibrils. *Angew. Chem. Int. Ed.* **2006**, *45*, 7324–7328. [[CrossRef](#)] [[PubMed](#)]
3. Sunde, M.; Serpell, L.C.; Bartlam, M.; Fraser, P.E.; Pepys, M.B.; Blake, C.C. Common core structure of amyloid fibrils by synchrotron X-ray diffraction. *J. Mol. Biol.* **1997**, *273*, 729–739. [[CrossRef](#)]
4. Karamanos, T.K.; Kalverda, A.P.; Thompson, G.S.; Radford, S.E. Mechanisms of amyloid formation revealed by solution NMR. *Prog. Nucl. Magn. Reson. Spectrosc.* **2015**, *88*, 86–104. [[CrossRef](#)]
5. Ferreira, S.T.; Vieira, M.N.; De Felice, F.G. Soluble protein oligomers as emerging toxins in Alzheimer's and other amyloid diseases. *IUBMB Life* **2007**, *59*, 332–345. [[CrossRef](#)] [[PubMed](#)]
6. Irvine, G.B.; El-Agnaf, O.M.; Shankar, G.M.; Walsh, D.M. Protein aggregation in the brain: The molecular basis for Alzheimer's and Parkinson's diseases. *Mol. Med.* **2008**, *14*, 451–464. [[CrossRef](#)] [[PubMed](#)]
7. Haataja, L.; Gurlo, T.; Huang, C.J.; Butler, P.C. Islet amyloid in type 2 diabetes, and the toxic oligomer hypothesis. *Endocr. Rev.* **2008**, *29*, 303–316. [[CrossRef](#)]
8. Chapman, M.R.; Robinson, L.S.; Pinkner, J.S.; Roth, R.; Heuser, J.; Hammar, M.; Normark, S.; Hultgren, S.J. Role of Escherichia coli curlin operons in directing amyloid fiber formation. *Science* **2002**, *295*, 851–855. [[CrossRef](#)]
9. Bayro, M.J.; Daviso, E.; Belenky, M.; Griffin, R.G.; Herzfeld, J. An amyloid organelle, solid-state NMR evidence for cross- $\beta$  assembly of gas vesicles. *J. Biol. Chem.* **2012**, *287*, 3479–3484. [[CrossRef](#)]
10. Mackay, J.P.; Matthews, J.M.; Winefield, R.D.; Mackay, L.G.; Haverkamp, R.G.; Templeton, M.D. The hydrophobin EAS is largely unstructured in solution and functions by forming amyloid-like structures. *Structure* **2001**, *9*, 83–91. [[CrossRef](#)]
11. Kenney, J.M.; Knight, D.; Wise, M.J.; Vollrath, F. Amyloidogenic nature of spider silk. *Eur. J. Biochem.* **2002**, *269*, 4159–4163. [[CrossRef](#)] [[PubMed](#)]
12. Fowler, D.M.; Koulov, A.V.; Alory-Jost, C.; Marks, M.S.; Balch, W.E.; Kelly, J.W. Functional amyloid formation within mammalian tissue. *PLoS Biol.* **2006**, *4*, e6. [[CrossRef](#)]
13. Li, J.; McQuade, T.; Siemer, A.B.; Napetschnig, J.; Moriwaki, K.; Hsiao, Y.-S.; Damko, E.; Moquin, D.; Walz, T.; McDermott, A. The RIP1/RIP3 necrosome forms a functional amyloid signaling complex required for programmed necrosis. *Cell* **2012**, *150*, 339–350. [[CrossRef](#)] [[PubMed](#)]
14. Maji, S.K.; Perrin, M.H.; Sawaya, M.R.; Jessberger, S.; Vadodaria, K.; Rissman, R.A.; Singru, P.S.; Nilsson, K.R.; Simon, R.; Schubert, D.; et al. Functional Amyloids As Natural Storage of Peptide Hormones in Pituitary Secretory Granules. *Science* **2009**, *325*, 328–332. [[CrossRef](#)]
15. Cohn, D.V.; Elting, J. Biosynthesis, processing, and secretion of parathormone and secretory protein-I. *Recent Prog. Horm. Res.* **1983**, *39*, 181–209.
16. Usdin, T.B. The PTH2 receptor and TIP39: A new peptide–receptor system. *Trends Pharmacol. Sci.* **2000**, *21*, 128–130. [[CrossRef](#)]
17. Guerreiro, P.M.; Renfro, J.L.; Power, D.M.; Canario, A.V. The parathyroid hormone family of peptides: Structure, tissue distribution, regulation, and potential functional roles in calcium and phosphate balance in fish. *Am. J. Physiol. Regul. Integr. Comp. Physiol.* **2007**, *292*, R679–R696. [[CrossRef](#)] [[PubMed](#)]
18. Freeman, M.W.; Wiren, K.M.; Rapoport, A.; Lazar, M.; Potts, J.T., Jr.; Kronenberg, H.M. Consequences of Amino-Terminal Deletions of Preproparathyroid Hormone Signal Sequence. *Mol. Endocrinol.* **1987**, *1*, 628–638. [[CrossRef](#)] [[PubMed](#)]
19. Wiren, K.M.; Potts, J.T., Jr.; Kronenberg, H.M. Importance of the propeptide sequence of human preproparathyroid hormone for signal sequence function. *J. Biol. Chem.* **1988**, *263*, 19771–19777. [[CrossRef](#)]
20. Gopalswamy, M.; Kumar, A.; Adler, J.; Baumann, M.; Henze, M.; Kumar, S.T.; Fändrich, M.; Scheidt, H.A.; Huster, D.; Balbach, J. Structural characterization of amyloid fibrils from the human parathyroid hormone. *Biochim. Biophys. Acta (BBA)-Proteins Proteom.* **2015**, *1854*, 249–257. [[CrossRef](#)]
21. Friedlander, G.; Amiel, C. Cellular mode of action of parathyroid hormone. *Adv. Nephrol. Necker Hosp.* **1994**, *23*, 265–279. [[PubMed](#)]
22. Martin, T.J.; Sims, N.A.; Seeman, E. Physiological and Pharmacological Roles of PTH and PTHrP in Bone using their Shared Receptor, PTH1R. *Endocr. Rev.* **2021**, *42*, 383–406. [[CrossRef](#)] [[PubMed](#)]
23. Mosekilde, L.; Søgaard, C.; Danielsen, C.; Tørring, O.; Nilsson, M. The anabolic effects of human parathyroid hormone (hPTH) on rat vertebral body mass are also reflected in the quality of bone, assessed by biomechanical testing: A comparison study between hPTH-(1–34) and hPTH-(1–84). *Endocrinology* **1991**, *129*, 421–428. [[CrossRef](#)]
24. Evgrafova, Z.; Voigt, B.; Roos, A.H.; Hause, G.; Hinderberger, D.; Balbach, J.; Binder, W.H. Modulation of amyloid  $\beta$  peptide aggregation by hydrophilic polymers. *Phys. Chem. Chem. Phys.* **2019**, *21*, 20999–21006. [[CrossRef](#)] [[PubMed](#)]
25. Evgrafova, Z.; Voigt, B.; Baumann, M.; Stephani, M.; Binder, W.H.; Balbach, J. Probing Polymer Chain Conformation and Fibril Formation of Peptide Conjugates. *ChemPhysChem* **2019**, *20*, 236–240. [[CrossRef](#)] [[PubMed](#)]
26. Evgrafova, Z.; Rothmund, S.; Voigt, B.; Hause, G.; Balbach, J.; Binder, W.H. Synthesis and Aggregation of Polymer-Amyloid  $\beta$  Conjugates. *Macromol. Rapid Commun.* **2020**, *41*, 1900378. [[CrossRef](#)] [[PubMed](#)]
27. Funtan, S.; Evgrafova, Z.; Adler, J.; Huster, D.; Binder, W.H. Amyloid Beta Aggregation in the Presence of Temperature-Sensitive Polymers. *Polymers* **2016**, *8*, 178. [[CrossRef](#)]
28. Hull, K.; Morstein, J.; Trauner, D. In Vivo Photopharmacology. *Chem. Rev.* **2018**, *118*, 10710–10747. [[CrossRef](#)]

29. Volgraf, M.; Gorostiza, P.; Numano, R.; Kramer, R.H.; Isacoff, E.Y.; Trauner, D. Allosteric control of an ionotropic glutamate receptor with an optical switch. *Nat. Chem. Biol.* **2006**, *2*, 47–52. [[CrossRef](#)]
30. Samanta, S.; Qin, C.; Lough, A.J.; Woolley, G.A. Bidirectional photocontrol of peptide conformation with a bridged azobenzene derivative. *Angew. Chem. Int. Ed.* **2012**, *51*, 6452–6455. [[CrossRef](#)]
31. Lindgren, N.J.V.; Varedian, M.; Gogoll, A. Photochemical Regulation of an Artificial Hydrolase by a Backbone Incorporated Tertiary Structure Switch. *Chem. Eur. J.* **2009**, *15*, 501–505. [[CrossRef](#)] [[PubMed](#)]
32. Schadendorf, T.; Hoppmann, C.; Rück-Braun, K. Synthesis of rigid photoswitchable hemithioindigo  $\omega$ -amino acids. *Tetrahedron Lett.* **2007**, *48*, 9044–9047. [[CrossRef](#)]
33. Lougheed, T.; Borisenko, V.; Hennig, T.; Ruck-Braun, K.; Woolley, G.A. Photomodulation of ionic current through hemithioindigo-modified gramicidin channels. *Org. Biomol. Chem.* **2004**, *2*, 2798–2801. [[CrossRef](#)] [[PubMed](#)]
34. Albert, L.; Peñalver, A.; Djokovic, N.; Werel, L.; Hoffarth, M.; Ruzic, D.; Xu, J.; Essen, L.O.; Nikolic, K.; Dou, Y. Modulating Protein–Protein Interactions with Visible-Light-Responsive Peptide Backbone Photoswitches. *ChemBioChem* **2019**, *20*, 1417–1429. [[CrossRef](#)]
35. Pozhidaeva, N.; Cormier, M.-E.; Chaudhari, A.; Woolley, G.A. Reversible photocontrol of peptide helix content: Adjusting thermal stability of the cis state. *Bioconjug. Chem.* **2004**, *15*, 1297–1303. [[CrossRef](#)]
36. Broichhagen, J.; Podewin, T.; Meyer-Berg, H.; Von Ohlen, Y.; Johnston, N.R.; Jones, B.J.; Bloom, S.R.; Rutter, G.A.; Hoffmann-Röder, A.; Hodson, D.J. Optical control of insulin secretion using an incretin switch. *Angew. Chem. Int. Ed.* **2015**, *54*, 15565–15569. [[CrossRef](#)]
37. Zhang, Y.; Erdmann, F.; Fischer, G. Augmented photoswitching modulates immune signaling. *Nat. Chem. Biol.* **2009**, *5*, 724–726. [[CrossRef](#)]
38. Hoppmann, C.; Schmieder, P.; Domaing, P.; Vogelreiter, G.; Eichhorst, J.; Wiesner, B.; Morano, I.; Rück-Braun, K.; Beyermann, M. Photocontrol of contracting muscle fibers. *Angew. Chem. Int. Ed.* **2011**, *50*, 7699–7702. [[CrossRef](#)]
39. Zhang, F.; Timm, K.A.; Arndt, K.M.; Woolley, G.A. Photocontrol of coiled-coil proteins in living cells. *Angew. Chem. Int. Ed.* **2010**, *49*, 3943–3946. [[CrossRef](#)]
40. Aemissegger, A.; Kräutler, V.; van Gunsteren, W.F.; Hilvert, D. A photoinducible  $\beta$ -hairpin. *J. Am. Chem. Soc.* **2005**, *127*, 2929–2936. [[CrossRef](#)]
41. Yeoh, Y.Q.; Yu, J.; Polyak, S.W.; Horsley, J.R.; Abell, A.D. Photopharmacological Control of Cyclic Antimicrobial Peptides. *ChemBioChem* **2018**, *19*, 2591–2597. [[CrossRef](#)]
42. Rück-Braun, K.; Kempa, S.; Priewisch, B.; Richter, A.; Seedorff, S.; Wallach, L. Azobenzene-Based  $\omega$ -Amino Acids and Related Building Blocks: Synthesis, Properties, and Application in Peptide Chemistry. *Synthesis* **2009**, *24*, 4256–4267. [[CrossRef](#)]
43. Ahmed, M.; Davis, J.; Aucoin, D.; Sato, T.; Ahuja, S.; Aimoto, S.; Elliott, J.I.; Van Nostrand, W.E.; Smith, S.O. Structural conversion of neurotoxic amyloid- $\beta$  1–42 oligomers to fibrils. *Nat. Struct. Mol. Biol.* **2010**, *17*, 561–567. [[CrossRef](#)] [[PubMed](#)]
44. Der-Sarkissian, A.; Jao, C.C.; Chen, J.; Langen, R. Structural organization of  $\alpha$ -synuclein fibrils studied by site-directed spin labeling. *J. Biol. Chem.* **2003**, *278*, 37530–37535. [[CrossRef](#)] [[PubMed](#)]
45. Makin, O.S.; Serpell, L.C. Structural characterisation of islet amyloid polypeptide fibrils. *J. Mol. Biol.* **2004**, *335*, 1279–1288. [[CrossRef](#)]
46. Murawska, G.M.; Poloni, C.; Simeth, N.A.; Szymanski, W.; Feringa, B.L. Comparative Study of Photoswitchable Zinc-Finger Domain and AT-Hook Motif for Light-Controlled Peptide–DNA Binding. *Chem. Eur. J.* **2019**, *25*, 4965–4973. [[CrossRef](#)]
47. Bandara, H.M.D.; Burdette, S.C. Photoisomerization in different classes of azobenzene. *Chem. Soc. Rev.* **2012**, *41*, 1809–1825. [[CrossRef](#)]
48. LeVine, H., III. [18] Quantification of  $\beta$ -sheet amyloid fibril structures with thioflavin T. In *Methods in Enzymology*; Elsevier: Amsterdam, The Netherlands, 1999; Volume 309, pp. 274–284.
49. Deike, S.; Rothmund, S.; Voigt, B.; Samantray, S.; Strodel, B.; Binder, W.H.  $\beta$ -Turn mimetic synthetic peptides as amyloid- $\beta$  aggregation inhibitors. *Bioorg. Chem.* **2020**, *101*, 104012. [[CrossRef](#)]
50. Ren, B.; Zhang, Y.; Zhang, M.; Liu, Y.; Zhang, D.; Gong, X.; Feng, Z.; Tang, J.; Chang, Y.; Zheng, J. Fundamentals of cross-seeding of amyloid proteins: An introduction. *J. Mater. Chem. B* **2019**, *7*, 7267–7282. [[CrossRef](#)]
51. Mulatihan, D.; Guo, T.; Zhao, Y. Azobenzene photoswitch for isomerization-dependent cancer therapy via azo-combretastatin A4 and phototretate. *Photochem. Photobiol.* **2020**, *96*, 1163–1168. [[CrossRef](#)]
52. Williams, R. Hepatic metabolism of drugs. *Gut* **1972**, *13*, 579. [[CrossRef](#)] [[PubMed](#)]
53. Álvarez, Z.; Kolberg-Edelbrock, A.N.; Sasselli, I.R.; Ortega, J.A.; Qiu, R.; Syrgiannis, Z.; Mirau, P.A.; Chen, F.; Chin, S.M.; Weigand, S.; et al. Bioactive scaffolds with enhanced supramolecular motion promote recovery from spinal cord injury. *Science* **2021**, *374*, 848–856. [[CrossRef](#)] [[PubMed](#)]